

RESEARCH ARTICLE

10.1002/2016GC006573

Key Points:

- Geochemistry of Eocene lacustrine sediments from the Fushun Basin are analyzed
- The regional climatic and environmental change is correlated with the global climate change
- The EECO is associated with extreme continental weathering and high lake productivity

Supporting Information:

- Supporting Information S1
- Data Set S1

Correspondence to:

Z. Chen,
chenzl@mail.iggcas.ac.cn

Citation:

Chen, Z., Z. Ding, Z. Tang, S. Yang, X. Wang, and L. Cui (2017), Paleoweathering and paleoenvironmental change recorded in lacustrine sediments of the early to middle Eocene in Fushun Basin, Northeast China, *Geochem. Geophys. Geosyst.*, 18, 41–51, doi:10.1002/2016GC006573.

Received 3 AUG 2016

Accepted 30 NOV 2016

Accepted article online 20 DEC 2016

Published online 10 JAN 2017

Paleoweathering and paleoenvironmental change recorded in lacustrine sediments of the early to middle Eocene in Fushun Basin, Northeast China

Zuoling Chen ¹, Zhongli Ding¹, Zihua Tang¹, Shiling Yang¹, Xu Wang¹, and Linlin Cui¹

¹Key Laboratory of Cenozoic Geology and Environment, Institute of Geology and Geophysics, Chinese Academy of Sciences, Beijing, China

Abstract Deciphering the long-term interaction among continental silicate weathering, global climate, and atmospheric CO₂ concentrations is helpful in understanding the mechanisms of the Cenozoic climate change and accessing the future climatic and environmental response to anthropogenic carbon emissions. The Eocene, which is characterized by the Early Eocene Climatic Optimum (EECO) and the following global cooling, represents an ideal test case. Here we generate geochemical data of the Eocene lacustrine sediments from the Fushun Basin, northeast China, to explore the regional climatic response to the global climate change. The chemical index of alteration (CIA) and plagioclase index of alteration (PIA) consistently show a gradual, long-term decrease, indicating a climatic transition from warm and humid to relatively cold and arid during the Eocene in the Fushun Basin. This climatic trend is broadly coincident with the global cooling and decreasing CO₂ concentration, implying that the regional climate is closely correlated with the global climate change over geological time scales. Additionally, the extreme silicate weathering and high lake productivity as reflected by relatively positive $\delta^{13}\text{C}$ values of lacustrine organic matter are associated with the EECO. This consistency may demonstrate that enhanced continental weathering and lake productivity had served as effective sinks to lower atmospheric CO₂ across the EECO. Collectively, our new geochemical data add supporting evidence for a long-term, close coupling among continental silicate weathering, climate, and global carbon cycle during the Eocene.

1. Introduction

The Earth's climate had undergone dramatic changes during the Cenozoic, characterized by a prominent transition from a warm, ice-free "greenhouse" world to a cool "icehouse" world with significant glaciations in the Antarctic continent [Zachos *et al.*, 2001, 2008]. Deep water temperatures determined from the stacked benthic oxygen isotope record [Zachos *et al.*, 2001, 2008] suggest that global climate experienced the Early Eocene Climatic Optimum (EECO; 52–49 Ma), which was the warmest period of the Cenozoic, as manifested by multiple-proxy mean annual temperature reconstructions for sea and land surfaces [Inglis *et al.*, 2015; Pancost *et al.*, 2013]. A progressive long-term cooling trend ensued over the middle and late Eocene epoch, and eventually caused continental ice sheet development in Antarctica at the Eocene/Oligocene boundary (~34 Ma) [Miller *et al.*, 1991; Zachos *et al.*, 2001]. The EECO has been ascribed to enhanced greenhouse effects causally linked to high atmospheric *p*CO₂ levels in response to increased volcanic emissions [Zachos *et al.*, 2008; Anagnostou *et al.*, 2016]. The subsequent persistent cooling has been attributed to decreased atmospheric *p*CO₂ levels, as evidenced by copious paleo-*p*CO₂ reconstruction [Lowenstein and Demicco, 2006; Beerling and Royer, 2011]. However, what caused the end of the EECO and the long-term decrease in *p*CO₂ during the middle Eocene is unclear [Thomas *et al.*, 2006]. A remarkable increase in atmospheric *p*CO₂ levels would lead to global warming through the greenhouse effect, thereby affecting global and regional hydrological cycles [Trenberth, 2011; Pierrehumbert, 2002], and thus conspire to enhance continental silicate weathering. An accelerated silicate chemical weathering would in turn sequester the carbon in marine sediments and reduce the *p*CO₂ concentration in the atmosphere through a negative feedback [Walker *et al.*, 1981]. Therefore, one of the possibilities proposed for this decrease in atmospheric *p*CO₂ concerns to an increase in silicate chemical weathering rate. The change of chemical weathering at past warm periods has been investigated using various methodologies; however, the results have been inconsistent. A widespread

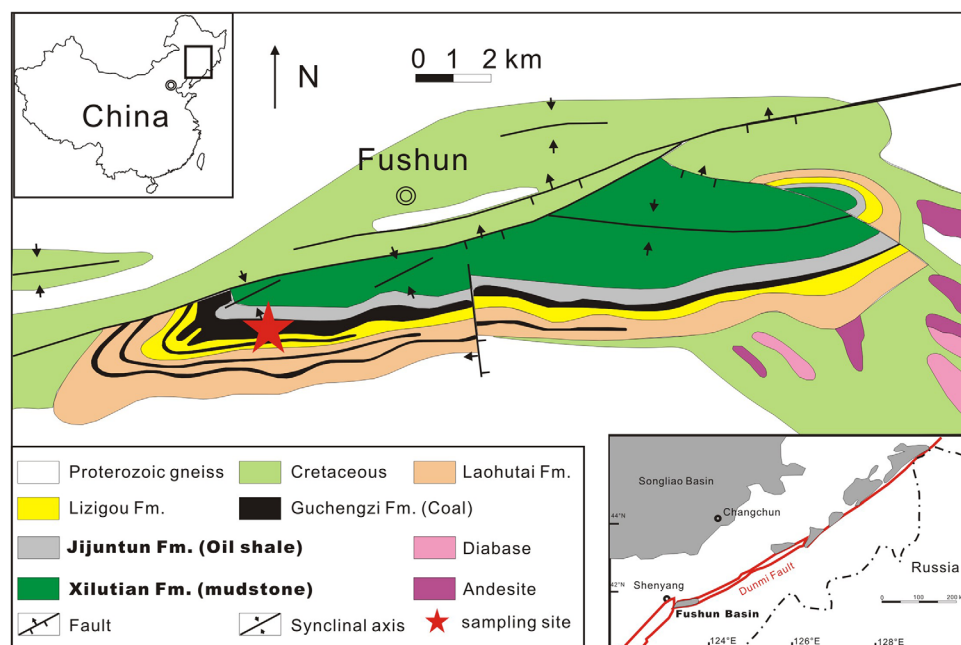


Figure 1. Geological map of Fushun Basin, Liaoning Province, Northeast China with location of the sampling site and the DunMi Fault shown as insert. The map is modified from Meng *et al.* [2012].

increase in kaolinite content has been observed during the PETM in terrestrial and marine sites worldwide [Robert and Kennett, 1994; John *et al.*, 2008; Chen *et al.*, 2016]. Some researchers ascribe the kaolinite peak to an increased chemical weathering in response to the PETM warming [Robert and Kennett, 1994; Chen *et al.*, 2016], while others explain it as a signal of enhanced exhumation and reworking of ancient kaolinite-rich soils [Thiry and Dupuis, 2000; John *et al.*, 2012]. In addition, the $^{87}\text{Sr}/^{86}\text{Sr}$ values of marine carbonates, which was explained as a proxy for global chemical weathering, do not show marked change from 50 to 40 Ma [Richter *et al.*, 1992]. But the use of the marine $^{87}\text{Sr}/^{86}\text{Sr}$ record as an ideal proxy for continental silicate weathering has been questioned because its values are influenced by many factors [Quade *et al.*, 1997]. In contrast, sedimentological records from North America and marine Li isotope provide evidence for an elevated silicate chemical weathering across the EECO [Smith *et al.*, 2008; Misra and Froelich, 2012]. Under these circumstances, additional methods to estimate the continental weathering and environmental change across the Eocene will be helpful to evaluate hypotheses concerning the interaction among climate change, chemical weathering, and carbon cycling.

Lacustrine sediments represent an ideal archive for reconstructing the environmental conditions that prevailed during lake evolution, and can provide significant information for the local and regional response to global climate change. Herein, we generate new geochemical records of the Eocene lacustrine mudstone and oil shale from the Fushun Basin, discuss paleoweathering and paleoenvironmental changes during the early Eocene to middle Eocene, and further assess regional responses to global change.

2. Materials and Methods

2.1. Geological Setting and Age Constraint

The Fushun Basin, located along the Dunhua-Mishan (DunMi) fault zone (Figure 1), is a small terrestrial strike-slip fault basin which formed on the basement of Proterozoic gneiss during the Paleogene faulted depression cycle [Wu *et al.*, 2002]. The basin fill comprises, in ascending order, the Paleocene Laohutai and Lizigou Formations and the Eocene Guchengzi, Jijuntun, and Xilutian Formations [Hong *et al.*, 1980]. All these formations are well exposed in the West Opencast Coalmine (41°50′35.0″N, 123°55′01.1″E). In this study, we focused principally on the Eocene Jijuntun and Xilutian Formations and collected samples at an interval of 1 m. The Jijuntun Formation, ~170 m thick, is composed of thick oil shale with interbedded carbonaceous shale and mudstone. The oil shale-bearing succession was deposited in rapidly subsiding

freshwater lake. It has been suggested that the depth of the lake increased during deposition of the Jijuntun Formation and the upper part of the Jijuntun Formation accumulated in a deep lake environment [Hong *et al.*, 1980]. The Xilutian Formation, ~430 m thick, consists of a set of thick green mudstones intercalated by silty argillite deposited in a shallow lake setting [Hong *et al.*, 1980].

The chronostratigraphic framework for the studied interval was roughly constrained based on magneto- and bio-stratigraphy, as well as the carbon isotope stratigraphy of the underlying coal seams [Hong *et al.*, 1980; Zhao *et al.*, 1994; Chen *et al.*, 2014]. The analyzed sequence spans the period circa 52–39 Ma. The studied interval covers the EECO and the middle Eocene cooling period, and thus provides an opportunity to assess regional response to global climate.

2.2. Major and Trace Elements Analyses

In total, 55 mudstone and oil shale samples were selected for major and trace elements analysis from the Fushun Basin, northeast China. All the samples were first finely ground in an agate mortar, then treated with 1 mol/L acetic acid to remove carbonate, and dried at 105°C. For major and trace elements analyses, about 0.5 g of carbonate-free sample powder was heated to 1000°C in a muffle furnace to determine the loss on ignition (LOI). The residue was then mixed with 5 g of $\text{Li}_2\text{B}_4\text{O}_7$ and fused to bead in a platinum crucible. The prepared discs were analyzed on a Shimadzu XRF-1500 for major and trace element contents at the Institute of Geology and Geophysics, CAS. Analytical uncertainties are better than 5% for all major elements based on replicate measurements of standards except MnO and P_2O_5 for which uncertainties can be up to $\pm 10\%$.

2.3. Organic Carbon and C/N Analyses

The total organic carbon (TOC) and total nitrogen (TN) were measured with a carbon-nitrogen-sulphur analyzer (Elementar Vario max C, Germany) after 1 mol/L HCl acid digestion to remove carbonates at the Institute of Tibetan Plateau Research, CAS. Measurement precision is better than 0.5% for both carbon and nitrogen. The values of TOC and TN, given in wt %, were used to calculate the C/N ratio by multiplying with the ratio of the atomic weights of carbon and nitrogen.

2.4. Organic Carbon Isotope ($\delta^{13}\text{C}_{\text{TOC}}$) Analyses

A total of 112 bulk samples were collected for stable isotope analyses of total organic carbon. They were powdered in an agate mortar and treated with 1 mol/L HCl to remove carbonate. The acid-insoluble fraction was then rinsed with distilled water, and dried at 50°C in an oven. Isotopic measurements were carried out on the acid-insoluble fraction using a Flash EA 1112 elemental analyzer, connected to a Finnigan MAT 253 mass spectrometer at the Institute of Geology and Geophysics, CAS. $\delta^{13}\text{C}_{\text{TOC}}$ values are reported relative to the international Pee Dee belemnite (PDB) standard (Vienna PDB). Analytical precision for individual analyses is better than $\pm 0.2\%$ based on replicate measurements of standards.

3. Results

3.1. Major Elements Geochemistry

Figure 2 shows the stratigraphic profile of major elements measured in this study along with the lithology. The carbonate-free samples are mainly composed of SiO_2 (39–77%), Al_2O_3 (6–22%), TFe_2O_3 (1–7%), K_2O (0.7–4.3%), and MgO (0.3–3.1%), with low content of TiO_2 (<1.5%), MnO (<0.1%), CaO (<0.4%), and Na_2O (<1.5%). Especially, the content of CaO (<0.4%) is far lower than the upper continental crust (UCC) [Taylor and McLennan, 1985] over the whole section. SiO_2 and TiO_2 generally lack significant variations across the section. The content of Al_2O_3 displays a gradual decrease in trend upward, with small fluctuations. In contrast, TFe_2O_3 , MgO , CaO , Na_2O , and K_2O consistently show an overall increasing trend upward throughout the sequence, with minimum values in the Jijuntun Formation.

3.2. Total Organic Carbon (TOC), C/N, and $\delta^{13}\text{C}_{\text{TOC}}$

The TOC concentration varies between 0.1% and 15% (Figure 3). It shows a gradual increasing trend from 50 to 150 m, and reaches the highest values (15%) at the upper of the Jijuntun Formation. Sediments deposited in the Xilutian Formation have relatively low TOC concentration, with fluctuation around 2%. The TOC/TN (C/N) ratios range from 1 to 21 (Figure 3) and are used here as proxy to identify the source of the organic matter deposited in the basin. Except two samples at 172.12 and 352.12 m, the rest of the section

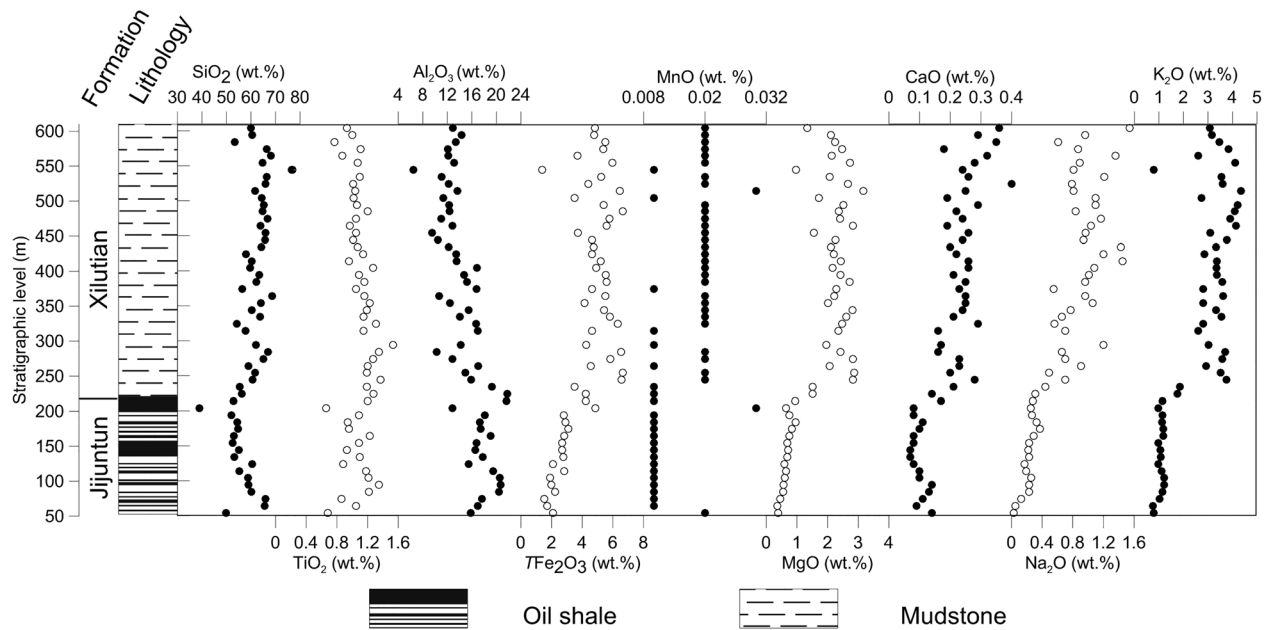


Figure 2. The stratigraphic profile of major elements for carbonate-free samples collected from the study section.

has C/N values below 20. The overall C/N trend is similar to that of TOC, with high values occurring in the Jijuntun Formation.

The $\delta^{13}\text{C}_{\text{TOC}}$ values fluctuate between -31‰ and -23.3‰ with significant variations throughout the sequence (Figure 3). These data generally display a negative trend from the base to the top of the section, punctuated by three positive shifts. The first markedly less negative $\delta^{13}\text{C}_{\text{TOC}}$ values ($\sim -26\text{‰}$) are observed

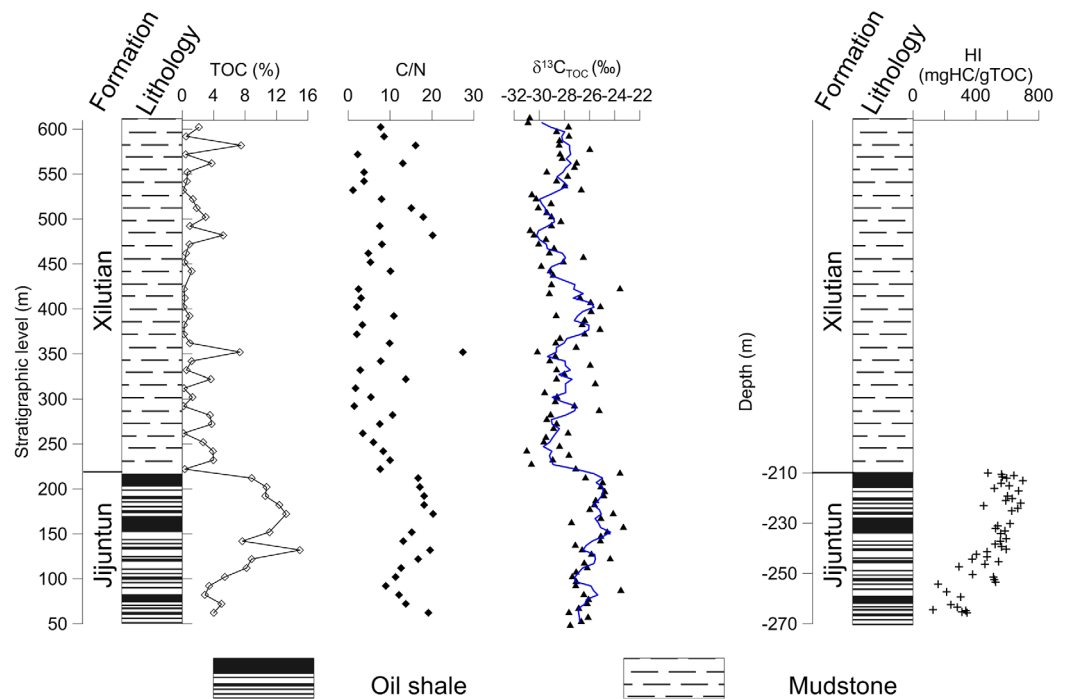


Figure 3. The stratigraphic profile of TOC, C/N, and $\delta^{13}\text{C}_{\text{TOC}}$. The HI values [Strobl *et al.*, 2014] in the Jijuntun Formation are also shown in depth profile. The blue solid line shows the three-point running average of $\delta^{13}\text{C}_{\text{TOC}}$ values.

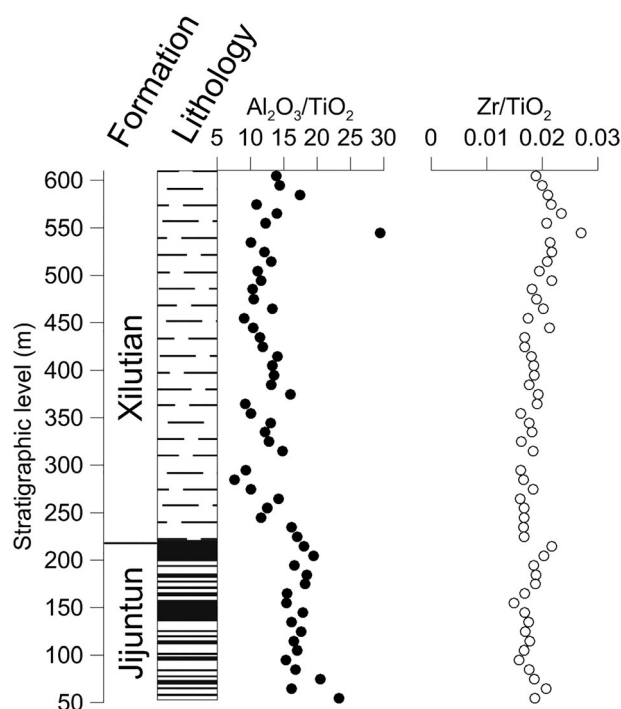


Figure 4. The stratigraphic profile of $\text{Al}_2\text{O}_3/\text{TiO}_2$ and Zr/TiO_2 .

become the majority of the detrital components in lacustrine sediments. Therefore, the element contents and ratios in lacustrine sediments can be served as proxies for the intensity of silicate chemical weathering in the source areas, and enable the reconstruction of paleoclimatic and paleoenvironmental changes. In addition to chemical weathering, diagenesis, provenance changes, and hydraulic sorting probably influence major element compositions [Fralick and Kronberg, 1997; Yang et al., 2006]. In general, diagenesis occurs at burial depths exceeding 2 km [Chamley, 1998]. The total thickness of the Cenozoic deposits in the Fushun Basin, however, is less than 2 km, implying that sediments did not suffer from significant deep burial diagenesis. Therefore, the effect of diagenesis on geochemical compositions, which could not be completely excluded, is considered to be insignificant in this study. During the weathering of source rocks, Al and Ti can be treated as essentially immobile elements due to the low solubility of the oxides and hydroxides of these elements in low-temperature aqueous solution [Hayashi et al., 1997]; in theory, the $\text{Al}_2\text{O}_3/\text{TiO}_2$ ratios should inherit the information of source rocks and thus have been widely used as an indicator of provenance [Hayashi et al., 1997]. With the exception of two samples, all $\text{Al}_2\text{O}_3/\text{TiO}_2$ values range from 8 to 21 (Figure 4), indicating that intermediate rocks constitute the source rocks [Hayashi et al., 1997] and the sediment source is relatively stable over the studied interval. Additionally, the high field strength element Zr is mainly associated with the heavy mineral fraction of sediments, and generally considered as one of the most immobile phases among the trace elements during chemical weathering. Hence, the Zr/TiO_2 ratios are widely used as an indicator of provenance rock types [Scheffler et al., 2003, 2006; Zhou et al., 2015]. The constant Zr/TiO_2 ratios around 0.02 are further suggestive of a relatively stable provenance rock during the studied period (Figure 4). Given that the sediments are mainly composed of fine-grained mudstone and shales, sedimentary sorting is not likely to be the determinant factor in controlling the element ratios [Nesbitt and Young, 1982]. Therefore, we conclude that the changes in major elements and their ratios are not caused by changes in provenance or transport processes, but mainly reflect the chemical weathering intensity in the watershed around the paleolake.

Here we evaluate the silicate chemical weathering information in the Fushun Basin using the selected elemental ratios. A good measure of the degree of chemical weathering can be obtained by calculating the chemical index of alteration (CIA) using molecular proportions of major elements [Nesbitt and Young, 1982]: $\text{CIA} = 100 * [\text{Al}_2\text{O}_3 / (\text{Al}_2\text{O}_3 + \text{CaO}^* + \text{Na}_2\text{O} + \text{K}_2\text{O})]$, where CaO^* is the amount of CaO incorporated in the silicate fraction of the rock. The weathering trend can be illustrated on an Al_2O_3 -($\text{CaO}^* + \text{Na}_2\text{O}$)- K_2O (A-CN-K)

between 50 and 220 m in the Jijuntun Formation, corresponding to higher TOC content. The other two positive excursions of $\sim 2\%$ in amplitude occur around 400 and 570 m, respectively.

4. Discussion

4.1. Paleoweathering and Paleoclimatic Reconstruction in the Fushun Basin

Silicate chemical weathering in the source areas strongly affects the major elements geochemistry of fine-grained siliclastic sediments [Nesbitt and Young, 1982; Harnois, 1988; Fedo et al., 1995]. Along with intensified chemical weathering, primary silicate minerals (e.g., feldspar) are gradually degraded to secondary clay minerals (e.g., kaolinite and illite). This weathering process would lead to preferential removal of mobile cations (e.g., Ca^{2+} , Na^+ , and K^+) relative to stable residual constituents (Al^{3+} and Ti^{4+}) [Nesbitt and Young, 1982]. Weathering products are then washed into the catchments by runoff and

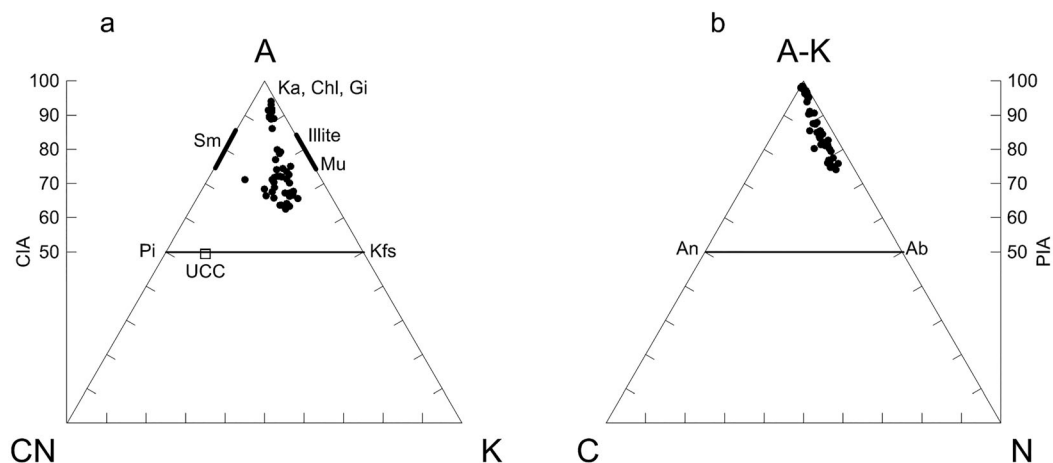


Figure 5. Triangular plots showing (a) molar proportions of Al_2O_3 -($\text{CaO}^* + \text{Na}_2\text{O}$)- K_2O in the A-CN-K diagram and (b) molar proportions of Al_2O_3 (subtracting the Al associated with K), CaO^* and Na_2O in the A-C-N diagram. The scales show the chemical index of alteration (CIA) and plagioclase index of alteration (PIA) values. UCC was also plotted as a reference. Pi, plagioclase; Kfs, K-feldspar; Sm, smectite; Ka, Kaolinite; Chl, chlorite; Gi, gibbsite; Mu, muscovite; An, anorthite; Ab, albite.

triangular plot [Nesbitt and Young, 1984, 1989]. The A-CN-K diagram displays a substantial loss of Ca, Na, and K in our section relative to UCC, as they tend to plot toward the A apex (Figure 5a). The CIA values of the fine-grained lacustrine sediments vary from 62 to 94, with an average of 77. Therefore, the positions of samples in the A-CN-K diagram, as well as their CIA values, indicate that these sediments were generated from source areas strongly affected by intense chemical weathering. The intensity of source weathering can also be assessed using the related plagioclase index of alteration (PIA): $\text{PIA} = 100 \cdot (\text{Al}_2\text{O}_3 - \text{K}_2\text{O}) / (\text{Al}_2\text{O}_3 + \text{CaO}^* + \text{Na}_2\text{O} - \text{K}_2\text{O})$, which quantifies the degree of destruction of plagioclase [Fedo et al., 1995]. A higher PIA value means a higher degree of plagioclase weathering. The PIA values range from 74 to 99, indicating an intermediate to intense weathering of plagioclase in source areas. The samples display low CaO^* values and plot along the A-N joint in the $(\text{Al}_2\text{O}_3 - \text{K}_2\text{O})$ - CaO^* - Na_2O triangular diagram (Figure 5b). This suggests that the sediments are almost depleted in anorthite and with increasing chemical weathering the sediments are gradually depleted in albite.

Stronger silicate chemical weathering is generally linked to warm temperatures and high precipitation, whereas more arid and cool conditions are generally associated with relatively weak chemical weathering [Nesbitt and Young, 1982]. As shown in Figure 6, the consistent trend of CIA and PIA clearly shows a gradual, long-term decreasing in chemical weathering intensity in the source areas; this suggests a climatic transition from warm and humid to relative cold and arid during the middle Eocene in the Fushun Basin, corresponding to the global cooling and decreasing $p\text{CO}_2$ [Zachos et al., 2008; Inglis et al., 2015; Beerling and Royer, 2011; Anagnostou et al., 2016]. In order to semiquantitatively estimate the regional paleoclimatic information, we here assume that the siliciclastic geochemistry of the mudstones in the lacustrine sedimentary successions semiquantitatively preserves the average paleoenvironmental signature of the soil mantle in the catchments around the Fushun Basin. It has been suggested that the intensity of chemical weathering and the degree of loss in labile elements in soil profiles are strongly depend on the prevailing climate [Sheldon et al., 2002; Nordt and Driese, 2010]. Based on stacked major elements data of North American soils, Sheldon et al. [2002] proposed two climofunctions to provide quantitative paleotemperature and precipitation reconstruction for paleosols. Recently, these climofunctions have been successfully applied to lacustrine and marine sediments for quantitative paleoclimatic estimate [Fantasia et al., 2016; Passchier et al., 2013]. Herein, we apply the similar method to semiquantitatively estimate mean annual precipitation (MAP) and mean annual temperature (MAT) values in the Fushun Basin, using CIA-K ($\text{CIA-K} = 100 \cdot \text{Al}_2\text{O}_3 / (\text{Al}_2\text{O}_3 + \text{CaO}^* + \text{Na}_2\text{O})$) and S ($S = (\text{K}_2\text{O} + \text{Na}_2\text{O}) / \text{Al}_2\text{O}_3$) indexes. The standard errors were $\pm 3.6^\circ\text{C}$ and ± 182 mm for MAT and MAP, respectively [Sheldon et al., 2002].

The calculated terrestrial MAT ranges from 6.9 to 16.3°C and MAP ranges from ~ 1000 to 1540 mm (Figure 6), in broad agreement with those derived from pollen assemblage within the limit of errors [Quan et al., 2011, 2012; Wang et al., 2010]. Overall, the MAT and MAP values present a gradual, long-term decrease in

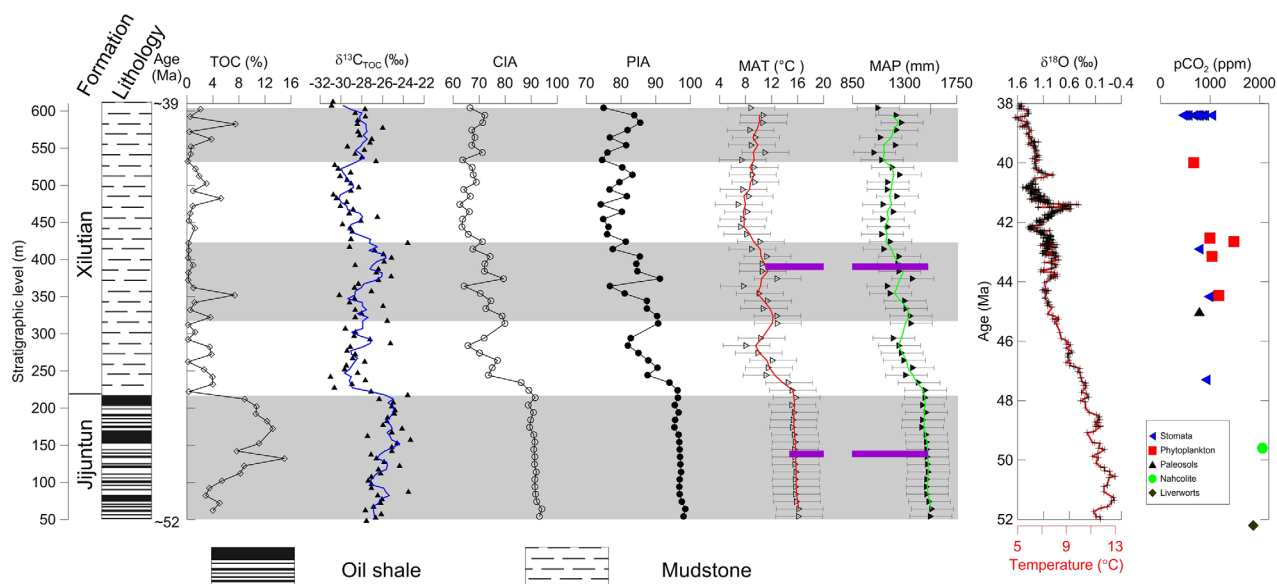


Figure 6. Comparison of regional paleoenvironmental and paleoclimatic information recorded in the Fushun Basin and the Eocene global climate ($\delta^{18}\text{O}$) recorded in marine sediments [Zachos *et al.*, 2008] as well as atmospheric pCO_2 [Beerling and Royer, 2011]. Gray shadings designate the periods of increased silicate weathering and lake productivity in the Fushun Basin. Mean annual temperature (MAT) and mean annual precipitation (MAP) are calculated from detrital geochemistry using climofunctions developed by Sheldon *et al.* [2002]. The purple bars indicate the ranges of MAT and MAP reconstructed from pollen assemblages in the Fushun Basin [Wang *et al.*, 2010]. The top and bottom age of the section are roughly constrained based on magneto- and bio-stratigraphy, as well as the carbon isotope stratigraphy of the underlying coal seams [Hong *et al.*, 1980; Zhao *et al.*, 1994; Chen *et al.*, 2014]. The blue (red and green) solid line shows the three-point running average of $\delta^{13}\text{C}_{\text{TOC}}$ (MAT and MAP) values.

trend from the base to the top of the section, in parallel with the Eocene global cooling [Zachos *et al.*, 2008] and decrease in atmospheric CO_2 concentrations [Beerling and Royer, 2011] (Figure 6). Evidence in support of the long-term regional climate change in the Fushun Basin has also come from the clay mineralogical composition, which records an obvious decrease in the content of kaolinite in lacustrine sediments during the Eocene [Meng *et al.*, 2012]. Together these results demonstrate that the regional climate is closely coupled with the global climate change over geological time scales.

Interestingly, the CIA and PIA record very high values between 50 and 220 m, during which both are above 90, indicating the degree of extreme chemical weathering [Fedo *et al.*, 1995]. Pollen studies of the Fushun Basin suggest that the paleoclimatic pattern follows a global trend, and recognize an interval of prominent increase in temperature in the lower part of Jijuntun Formation [Quan *et al.*, 2012]. In combination with carbon isotope stratigraphy of Guchengzi Formation [Chen *et al.*, 2014] and rough paleomagnetic results [Zhao *et al.*, 1994], the period of extreme weathering geochronologically corresponds to the Early Eocene Climatic Optimum (EECO), which was the warmest period of the Cenozoic. Warm temperatures and enhanced precipitation have been suggested as the primary factors that would intensify the silicate weathering [Walker *et al.*, 1981]. As a result, our results strongly support the existence of a climatic-continental silicate weathering feedback during the EECO.

4.2. $\delta^{13}\text{C}_{\text{TOC}}$ and Paleoproductivity

The organic geochemistry of lacustrine sediment generally provides significant information on the paleoenvironmental and paleoclimatic changes in lakes and their catchments. Many processes can potentially influence the $\delta^{13}\text{C}_{\text{TOC}}$ values of bulk lacustrine organic matter. Changes in bulk $\delta^{13}\text{C}_{\text{TOC}}$ values may be caused by different sources of carbon as well as change in lake productivity [Lücke *et al.*, 2003]. In general, the organic matter in the lacustrine sediments is mainly from wash-in land-derived plants (C3 or C4) and autochthonous planktonic algae. Since the earliest origins and expansion of C4 plants probably occurred after the Oligocene [Vicentini *et al.*, 2008; Tipple and Pagani, 2007], the potential sources for organic matter in the Eocene Fushun Basin are reduced to (1) detrital C3 land plants and (2) photosynthetic lacustrine algae (primary producers). However, lake-derived organic matter that is produced by phytoplankton (C3 algae) is isotopically indistinguishable from organic matter produced by C3 plants in the surrounding catchments [Meyers and Lallier-vergès, 1999]. Molar C/N ratios of land-derived plants are substantially higher than those of lacustrine

phytoplankton and thus change of organic matter source should be detectable by changes in sedimentary C/N ratios [Meyers, 1994; Meyers and Lallier-vergès, 1999]. The C/N ratios in the Xilutian Formation fluctuate around 10 and are well below 20, the threshold value diagnostic of land-derived organic matter (Figure 3) [Meyers, 1994]. These results imply that the prevailing source of sedimentary organic matter in the Xilutian Formation is autochthonous production. The high C/N ratios of close to 20 in the Jijuntun Formation appear to suggest a significant contribution of land-derived organic matter. The hydrogen index (HI) from Rock Eval pyrolysis (Figure 3), however, indicates a mixture of prevailing landplant-derived and algal material only occurring in the lowest part of the Jijuntun Formation, whereas the organic matter of the middle and upper part of the Jijuntun Formation is predominantly composed by type II to I kerogen of lacustrine algae origin [Strobl *et al.*, 2014]. In addition, the C/N ratios do not reveal a convincing correlation with the $\delta^{13}\text{C}_{\text{TOC}}$ values (Figure 3). Therefore, terrestrial organic matter input can be neglected as a major contribution to the change of $\delta^{13}\text{C}_{\text{TOC}}$ values during our investigated period except for the lowest part of the Jijuntun Formation. In general, increased accumulation of organic matter and its $\delta^{13}\text{C}$ value have been widely used as indicator of enhanced aquatic algae productivity in lakes [Brenner *et al.*, 1999]. The photosynthesis of phytoplankton preferentially utilizes ^{12}C of the dissolved inorganic carbon (DIC) source to produce organic matter [Wolfe *et al.*, 2001]. Along with increased lake productivity and subsequent burial of algal organic matter, the availability of DIC becomes enriched in ^{13}C , which then causes an increase in the $\delta^{13}\text{C}$ values of newly produced organic matter [Meyers, 2003]. We thus explain the positive anomalies recorded in the lacustrine bulk $\delta^{13}\text{C}_{\text{TOC}}$ values as the change in primary productivity of phytoplankton. Such relative positive excursions in $\delta^{13}\text{C}_{\text{TOC}}$ values have been documented in modern and ancient lacustrine sediments associated with high productivity, both seasonal and long-term scales [Hollander *et al.*, 1993; Schelske and Hodell, 1991]. In the Fushun Basin, the $\delta^{13}\text{C}_{\text{TOC}}$ values display an overall similar change in trend with the chemical weathering indexes (CIA and PIA). The positive shifts of $\delta^{13}\text{C}_{\text{TOC}}$ values broadly correspond to the relatively high weathering intensity. In general, higher temperature would increase the length of summer growing season and the intensity of chemical weathering in the catchment areas, leading to a greater flux of nutrients (P, Fe, and N) to the lake basin. The excessive nutrient availability and prolonged growing season would in turn enhance the lake productivity, causing the observed positive shifts of the $\delta^{13}\text{C}_{\text{TOC}}$ values. To summarize, our data imply a close coupling between continental weathering and lake productivity responding to global climate change. Especially, the period of extreme weathering during the EECO coincides with the most positive $\delta^{13}\text{C}_{\text{TOC}}$ values and the highest TOC content. Warmer and wetter climate as reflected by clay mineral composition and pollen assemblage [Meng *et al.*, 2012; Quan *et al.*, 2012] resulted in extreme silicate weathering and greater amount of land runoff which washed more nutrients into the lake, promoting lake productivity and subsequent burial of organic matter as oil shale in the Fushun Basin. This consistency indicates that the increased lake productivity and subsequent burial of organic matter may serve as a potential carbon sink to lower the atmosphere $p\text{CO}_2$ during the late early Eocene.

4.3. Implication for the Eocene Carbon Cycle

Over geologic time scales, atmospheric $p\text{CO}_2$ levels are principally controlled by carbon input to the ocean-atmosphere system from volcanic and metamorphic outgassing, as well as output through silicate weathering and organic carbon burial at the Earth's surface [Walker *et al.*, 1981; Berner and Caldeira, 1997]. The early Eocene is characterized by the EECO, which was the warmest interval of the past 65×10^6 years. It has been suggested that the EECO was most likely casually linked to an enhanced greenhouse effect due to higher atmospheric $p\text{CO}_2$ concentrations [Zachos *et al.*, 2008]. Paleo- $p\text{CO}_2$ reconstructions, based on multiple proxies, indeed record elevated CO_2 concentration during the EECO [Hyland and Sheldon, 2013; Beerling and Royer, 2011; Smith *et al.*, 2008; Anagnostou *et al.*, 2016]. These high $p\text{CO}_2$ levels have been attributed to increased CO_2 outgassing due to increased global seafloor spreading and the emplacement of the North Atlantic igneous province during the EECO [Miller *et al.*, 2005; Thomas and Bralower, 2005], or metamorphic outgassing related to the convergence of Greater India with Eurasia [Kent and Muttoni, 2008].

The pervasively accepted negative feedback processes, which stabilize the Earth's long-term climate and also functionally depend on the change in the atmospheric CO_2 concentrations, are the response of continental silicate weathering to climates and burial magnitude of organic carbon [Walker *et al.*, 1981; Kump *et al.*, 2000; Galy *et al.*, 2007]. In the Fushun Basin, the period of extreme silicate weathering geochronologically corresponds to the EECO (Figure 6). Similarly, the studies from North American and Antarctica show an elevated silicate weathering during the EECO [Smith *et al.*, 2008; Hyland and Sheldon, 2013; Dingle and

Lavelle, 1998]. Together these results suggest that the extreme weathering event during the EECO was a global event in response to elevated $p\text{CO}_2$ levels. Further evidence for the global weathering event comes from the marine Li isotope record, which shows the minimum $\delta^7\text{Li}$ values during the EECO [Misra and Froelich, 2012].

As a corollary, intensified silicate weathering will deliver plentiful nutrients (Fe, P, and N) to the lake by runoff, which in combination with prolonged growing season should promote lake productivity and accumulation of organic matter. Indeed, $\delta^{13}\text{C}_{\text{TOC}}$ and TOC values in the Fushun Basin reflect increased lake productivity and subsequent burial of organic matter as oil shales across the EECO (Figure 6). In fact, lacustrine oil shales with an early-middle Eocene age are widespread throughout the world, including the Parachute Creek Member of the Green River Formation in North America [Cumming et al., 2012], the Messel oil shale in Germany [Lenz et al., 2007], oil shales in central Jordan [Alqudah et al., 2014], China [Sun et al., 2013; Strobl et al., 2015], and Turkey [Oçakoğlu et al., 2012]. Because organic carbon is highly enriched in ^{12}C during photosynthesis, increased burial of organic matter will remove the ^{12}C and thus cause less depleted $\delta^{13}\text{C}$ in the exogenic carbon reservoir. The stacked marine $\delta^{13}\text{C}$ values record a gradual increase across the EECO [Zachos et al., 2008], coincident with abundant deposition of oil shales over the world. This consistency may demonstrate that the increased lake productivity had also acted as an effective sink for the atmospheric CO_2 .

After the EECO, the CIA and $\delta^{13}\text{C}_{\text{TOC}}$ values exhibit an overall decrease in trend, synchronous with the gradual decrease in $p\text{CO}_2$ [Beerling and Royer, 2011] and global temperature [Zachos et al., 2008] (Figure 6). This consistency demonstrates that the regional climate change correlates closely with the global cooling, and the deteriorated climate led to weak silicate weathering and decreasing lake productivity. In addition, the long-term decreasing trend is punctuated by two intervals with a bit high CIA and $\delta^{13}\text{C}_{\text{TOC}}$ values around 400 and 570 m, respectively (Figure 6). We speculate that they are likely associated with two other periods of warming. To sum up, our new data add supporting evidence for the close coupling among global climate, continental silicate weathering, and carbon cycling throughout the Eocene.

5. Conclusions

Geochemical proxies are analyzed for the Eocene fine-grained lacustrine sediment from the Fushun Basin, northeast China, in order to reveal the chemical weathering intensity in the source regions and the lake paleoproductivity. This provides useful information about regional environmental response to global climate change.

The CIA and PIA values generally present a gradual, long term decrease in the intensity of silicate weathering across the Eocene, indicating a decreasing of precipitation and temperature accompanying with the global cooling and gradual decline in atmospheric CO_2 . These results imply that the regional environment is closely correlated with the global climate change over geological time scales. The interval of extreme silicate weathering and high lake productivity geochronologically corresponds to the EECO, demonstrating that continental silicate chemical weathering and organic carbon burial have served as effective sinks to lower the atmospheric CO_2 . Collectively, our new geochemical data argue for the existence of a close coupling among continental silicate weathering, climate, and global carbon cycle during the Eocene.

Acknowledgments

This work was supported by the (973) National Basic Research Program of China (grant 2013CB956404), the Natural Science Foundation of China (grant 41502169), the Strategic Priority Research Program of the Chinese Academy of Sciences (grant XDB03020503), and the China Postdoctoral Science Foundation (grant 2015M570143). We thank Dingshui Xue and Licheng Guo for their assistance in data measurement and Shaohua Feng for the field sampling. We also thank two anonymous reviewers for their helpful comments. Data supporting the paper are available in supporting information.

References

- Alqudah, M., M. A. Hussein, O. G. Podlaha, S. van den Boorn, S. Kolonic, and J. Mutterlose (2014), Calcareous nannofossil biostratigraphy of Eocene oil shales from central Jordan, *GeoArabia*, 19, 117–140.
- Anagnostou, E., E. H. John, K. M. Edgar, G. L. Foster, A. Ridgwell, G. N. Inglis, R. D. Pancost, D. J. Lunt, and P. N. Pearson (2016), Changing atmospheric CO_2 concentration was the primary driver of early Cenozoic climate, *Nature*, 533, 380–384.
- Beerling, D. J., and D. L. Royer (2011), Convergent Cenozoic CO_2 history, *Nat. Geosci.*, 4, 418–420.
- Berner, R. A., and K. Caldeira (1997), The need for mass balance and feedback in the geochemical carbon cycle, *Geology*, 25, 955–956.
- Brenner, M., T. J. Whitmore, J. H. Curtis, D. A. Hodell, and C. L. Schelske (1999), Stable isotope ($\delta^{13}\text{C}$ and $\delta^{15}\text{N}$) signatures of sedimented organic matter as indicators of historic lake trophic state, *J. Paleolimnol.*, 22, 205–221.
- Chamley, H. (1998), Clay mineral sedimentation in the Ocean, in *Soils and Sediments (Mineralogy and Geochemistry)*, edited by H. Paquet and N. Clauer, pp. 269–302, Springer, Berlin.
- Chen, Z., Z. Ding, Z. Tang, X. Wang, and S. Yang (2014), Early Eocene carbon isotope excursions: Evidence from the terrestrial coal seam in the Fushun Basin, Northeast China, *Geophys. Res. Lett.*, 41, 3559–3564, doi:10.1002/2014GL059808.
- Chen, Z., Z. Ding, S. Yang, C. Zhang, and X. Wang (2016), Increased precipitation and weathering across the Paleocene-Eocene Thermal Maximum in central China, *Geochem. Geophys. Geosyst.*, 17, 2286–2297, doi:10.1002/2016GC006333.

- Cumming, V. M., D. Selby, and P. G. Lillis (2012), Re-Os geochronology of the lacustrine Green River Formation: Insights into direct depositional dating of lacustrine successions, Re-Os systematics and paleocontinental weathering, *Earth Planet. Sci. Lett.*, *359*, 194–205.
- Dingle, R. V., and M. Lavelle (1998), Late Cretaceous-Cenozoic climatic variations of the northern Antarctic Peninsula: New geochemical evidence and review, *Palaeogeogr. Palaeoclimatol. Palaeoecol.*, *141*, 215–232.
- Fantasia, A., T. Adatte, J. E. Spangenberg, and E. Font (2016), Palaeoenvironmental changes associated with Deccan volcanism, examples from terrestrial deposits from Central India, *Palaeogeogr. Palaeoclimatol. Palaeoecol.*, *441*, 165–180.
- Fedo, C. M., H. W. Nesbitt, and G. M. Young (1995), Unravelling the effects of potassium metasomatism in sedimentary rocks and paleosols, with implications for paleoweathering conditions and provenance, *Geology*, *23*, 921–924.
- Fralick, P. W., and B. I. Kronberg (1997), Geochemical discrimination of elastic sedimentary rock sources, *Sediment. Geol.*, *113*, 111–124.
- Galy, V., C. France-Lanord, O. Beysac, P. Faure, H. Kudrass, and F. Palhol (2007), Efficient organic carbon burial in the Bengal fan sustained by the Himalayan erosional system, *Nature*, *450*, 407–410.
- Harnois, L. (1988), The CIW index: A new chemical index of weathering, *Sediment. Geol.*, *55*, 319–322.
- Hayashi, K. I., H. Fujisawa, H. D. Holland, and H. Ohmoto (1997), Geochemistry of ~1.9 Ga sedimentary rocks from northeastern Labrador, *Can. Geochim. Cosmochim. Acta*, *61*, 4115–4137.
- Hollander, D. J., J. A. A. McKenzie, K. H. Hsu, and A. Y. Huc (1993), Application of an eutrophic lake model to the origin of ancient organic-carbon rich sediments, *Global Biogeochem. Cycle*, *7*, 157–179.
- Hong, Y., Z. Yang, S. Wang, X. Sun, N. Du, M. Sun, and Y. Li (1980), *A Research on the Strata and Palaeontology of the Fushun Coal Field in Liaoning Province*, pp. 1–99, Sci. Press, Beijing.
- Hyland, E. G., and N. D. Sheldon (2013), Coupled CO₂-climate response during the Early Eocene Climatic Optimum, *Palaeogeogr. Palaeoclimatol. Palaeoecol.*, *369*, 125–135.
- Inglis, G. N., et al. (2015), Descent toward the Icehouse: Eocene sea surface cooling inferred from GDGT distributions, *Paleoceanography*, *30*, 1000–1020, doi:10.1002/2014PA002723.
- John, C. M., S. M. Bohaty, J. C. Zachos, A. Sluijs, S. Gibbs, H. Brinkhuis, and T. J. Bralower (2008), North American continental margin records of the Paleocene-Eocene thermal maximum: Implications for global carbon and hydrological cycling, *Paleoceanography*, *23*, PA2217, doi:10.1029/2007PA001465.
- John, C. M., N. R. Banerjee, F. J. Longstaffe, C. Sica, K. R. Law, and J. C. Zachos (2012), Clay assemblage and oxygen isotopic constraints on the weathering response to the Paleocene-Eocene thermal maximum, east coast of North America, *Geology*, *40*, 591–594.
- Kent, D. V., and G. Muttoni (2008), Equatorial convergence of India and early Cenozoic climate trends, *Proc. Natl. Acad. Sci. U. S. A.*, *105*, 16,065–16,070.
- Kump, L. R., S. L. Brantley, and M. A. Arthur (2000), Chemical weathering, atmospheric CO₂, and climate, *Annu. Rev. Earth Planet. Sci.*, *28*, 611–667.
- Lenz, O. K., V. Wilde, and W. Riegel (2007), Recolonization of a Middle Eocene volcanic site: Quantitative palynology of the initial phase of the maar lake of Messel (Germany), *Rev. Palaeobot. Palynol.*, *145*, 217–242.
- Lowenstein, T. K., and R. V. Demicco (2006), Elevated Eocene atmospheric CO₂ and its subsequent decline, *Science*, *313*, 1928–1928.
- Lücke, A., G. H. Schleser, B. Zolitschka, and J. F. W. Negendank (2003), A Lateglacial and Holocene organic carbon isotope record of lacustrine palaeoproductivity and climatic change derived from varved lake sediments of Lake Holzmaar, Germany, *Quat. Sci. Rev.*, *22*, 569–580.
- Meng, Q., Z. Liu, A. A. Bruch, R. Liu, and F. Hu (2012), Palaeoclimatic evolution during Eocene and its influence on oil shale mineralization, Fushun basin, China, *J. Asian Earth Sci.*, *45*, 95–105.
- Meyers, P. A. (1994), Preservation of elemental and isotopic source identification of sedimentary organic matter, *Chem. Geol.*, *114*, 289–302.
- Meyers, P. A. (2003), Applications of organic geochemistry to paleolimnological reconstructions: A summary of examples from the Laurentian Great Lakes, *Org. Geochem.*, *34*, 261–289.
- Meyers, P. A., and E. Lallier-vergès (1999), Lacustrine sedimentary organic matter records of late Quaternary paleoclimates, *J. Paleolimnol.*, *21*, 345–372.
- Miller, K. G., J. D. Wright, and R. G. Fairbanks (1991), Unlocking the ice house: Oligocene-Miocene oxygen isotopes, eustasy, and margin erosion, *J. Geophys. Res.*, *96*, 6829–6848.
- Miller, K. G., M. A. Kominz, J. V. Browning, J. D. Wright, G. S. Mountain, M. E. Katz, P. J. Sugarman, B. S. Cramer, N. Christie-Blick, and S. F. Pekar (2005), The Phanerozoic record of global sea-level change, *Science*, *310*, 1293–1298.
- Misra, S., and P. N. Froelich (2012), Lithium isotope history of Cenozoic seawater: Changes in silicate weathering and reverse weathering, *Science*, *335*, 818–823.
- Nesbitt, H. W., and G. M. Young (1982), Early Proterozoic climates and plate motions inferred from major element chemistry of lutites, *Nature*, *299*, 715–717.
- Nesbitt, H. W., and G. M. Young (1984), Prediction of some weathering trends of plutonic and volcanic rocks based on thermodynamic and kinetic considerations, *Geochim. Cosmochim. Acta*, *48*, 1523–1534.
- Nesbitt, H. W., and G. M. Young (1989), Formation and diagenesis of weathering profiles, *J. Geol.*, *97*, 129–147.
- Nordt, L., and S. Driese (2010), A modern soil characterization approach to reconstructing physical and chemical properties of paleo-Vertisol, *Am. J. Sci.*, *310*, 37–64.
- Ocakoğlu, F., S. Açıkalın, İ. Ö. Yılmaz, Ü. Şafak, and C. Gökçeoğlu (2012), Evidence of orbital forcing in lake-level fluctuations in the Middle Eocene oil shale-bearing lacustrine successions in the Mudurnu-Göynük Basin, NW Anatolia (Turkey), *J. Asian Earth Sci.*, *56*, 54–71.
- Pancost, R. D., et al. (2013), Early Paleogene evolution of terrestrial climate in the SW Pacific, Southern New Zealand, *Geochem. Geophys. Geosyst.*, *14*, 5413–5429, doi:10.1002/2013GC004935.
- Passchier, S., S. M. Bohaty, F. Jiménez-Espejo, J. Pross, U. Röhl, T. van de Flierdt, C. Escutia, and H. Brinkhuis (2013), Early Eocene to middle Miocene cooling and aridification of East Antarctica, *Geochem. Geophys. Geosyst.*, *14*, 1399–1410, doi:10.1002/ggge.20106.
- Pierrehumbert, R. T. (2002), The hydrologic cycle in deep-time climate problems, *Nature*, *419*, 191–198.
- Quade, J., L. Roe, P. G. DeCelles, and T. P. Ojha (1997), The late Neogene ⁸⁷Sr/⁸⁶Sr record of lowland Himalayan Rivers, *Science*, *276*, 1828–1831.
- Quan, C., Y. Liu, and T. Utescher (2011), Paleogene evolution of precipitation in northeastern China supporting the middle Eocene intensification of the east Asian monsoon, *Palaio*, *26*, 743–753.
- Quan, C., Y. Liu, and T. Utescher (2012), Paleogene temperature gradient, seasonal variation and climate evolution of northeast China, *Palaeogeogr. Palaeoclimatol. Palaeoecol.*, *313*, 150–161.
- Richter, F. M., D. B. Rowley, and D. J. DePaolo (1992), Sr isotope evolution of seawater: The role of tectonics, *Earth Planet. Sci. Lett.*, *109*, 11–23.
- Robert, C., and J. P. Kennett (1994), Antarctic subtropical humid episode at the Paleocene-Eocene boundary: Clay - mineral evidence, *Geology*, *22*, 211–214.

- Scheffler, K., S. Hoernes, and L. Schwark (2003), Global changes during Carboniferous–Permian glaciation of Gondwana: Linking polar and equatorial climate evolution by geochemical proxies, *Geology*, *31*, 605–608.
- Scheffler, K., D. Buehmann, and L. Schwark (2006), Analysis of late Palaeozoic glacial to postglacial sedimentary successions in South Africa by geochemical proxies—Response to climate evolution and sedimentary environment, *Palaeogeogr. Palaeoclimatol. Palaeoecol.*, *240*, 184–203.
- Schelske, C. L., and D. A. Hodell (1991), Recent changes in productivity and climate of Lake Ontario detected by isotopic analysis of sediments, *Limnol. Oceanogr.*, *36*, 961–975.
- Sheldon, N. D., G. J. Retallack, and S. Tanaka (2002), Geochemical climofunction from North American soils and application to paleosols across the Eocene–Oligocene boundary in Oregon, *J. Geol.*, *110*, 687–696.
- Smith, M. E., A. C. Carroll, and E. R. Mueller (2008), Elevated weathering rates in the Rocky Mountains during the Early Eocene Climatic Optimum, *Nat. Geosci.*, *1*, 370–374.
- Strobl, S. A. I., R. F. Sachsenhofer, A. Bechtel, R. Gratzer, D. Gross, S. N. H. Bokhari, R. Liu, Z. Liu, Q. Meng, and P. Sun (2014), Depositional environment of oil shale within the Eocene Jijuntun Formation in the Fushun Basin (NE China), *Mar. Pet. Geol.*, *56*, 166–183.
- Strobl, S. A. I., R. F. Sachsenhofer, A. Bechtel, Q. Meng, and P. Sun (2015), Deposition of coal and oil shale in NE China: The Eocene Huadian Basin compared to the coeval Fushun Basin, *Mar. Pet. Geol.*, *64*, 347–362.
- Sun, P., R. F. Sachsenhofer, Z. Liu, S. A. I. Strobl, Q. Meng, R. Liu, and Z. Zhen (2013), Organic matter accumulation in the oil shale- and coal-bearing Huadian Basin (Eocene; NE China), *Int. J. Coal Geol.*, *105*, 1–15.
- Taylor, S. R., and S. M. McLennan (1985), *The Continental Crust: Its Composition and Evolution*, 312 pp., Blackwell, Malden, Mass.
- Thiry, M., and M. Dupuis (2000), Use of clay minerals for paleoclimatic reconstructions: Limits of the method with special reference to the Paleocene–lower Eocene interval, *GFF*, *122*, 166–167.
- Thomas, D. J., and T. J. Bralower (2005), Sedimentary trace element constraints on the role of North Atlantic Igneous Province volcanism in late Paleocene–early Eocene environmental change, *Mar. Geol.*, *217*, 233–254.
- Thomas, E., H. Brinkhuis, M. Huber, and U. Röhl (2006), An ocean view of the early Cenozoic greenhouse world, *Oceanography*, *19*, 63–72.
- Tipple, B. J., and M. Pagani (2007), The early origins of terrestrial C₄ photosynthesis, *Annu. Rev. Earth Planet. Sci.*, *35*, 435–461.
- Trenberth, K. E. (2011), Changes in precipitation with climate change, *Clim. Res.*, *47*, 1–16.
- Vicentini, A., J. C. Barber, S. S. Aliscioni, L. M. Giussani, and E. A. Kellogg (2008), The age of the grasses and clusters of origins of C₄ photosynthesis, *Global Change Biol.*, *14*, 2963–2977.
- Wang, Q., D. K. Ferguson, G. Feng, A. G. Ablaev, Y. Wang, J. Yang, Y. Li, and C. Li (2010), Climatic change during the Palaeocene to Eocene based on fossil plants from Fushun, China, *Palaeogeogr. Palaeoclimatol. Palaeoecol.*, *295*, 323–331.
- Walker, J. C. G., P. B. Hays, and J. F. Kasting (1981), A negative feedback mechanism for the long-term stabilization of Earth's surface temperature, *J. Geophys. Res.*, *86*, 9776–9782.
- Wolfe, B. B., T. W. D. Edwards, K. R. M. Beuning, and R. J. Elgood (2001), Carbon and oxygen isotope analysis of lake sediment cellulose: methods and applications, in *Tracking Environmental Changes Using Lake Sediments: Physical and Chemical Techniques*, edited by W. M. Last and J. P. Smol, pp. 373–400, Kluwer, Dordrecht, Netherlands.
- Wu, C., X. Wang, G. Liu, S. Li, X. Mao, and X. Li (2002), Study on dynamics of tectonics evolution in the Fushun Basin, Northeast China, *Sci. China Ser. D*, *45*, 311–324.
- Yang, S. L., F. Ding, and Z. L. Ding (2006), Pleistocene chemical weathering history of Asian arid and semi-arid regions recorded in loessdeposits of China and Tajikistan, *Geochim. Cosmochim. Acta*, *70*, 1695–1709.
- Zachos, J., M. Pagani, L. Sloan, E. Thomas, and K. Billups (2001), Trends, rhythms, and aberrations in global climate 65 Ma to present, *Science*, *292*, 686–693.
- Zachos, J. C., G. R. Dickens, and R. E. Zeebe (2008), An early Cenozoic perspective on greenhouse warming and carbon-cycle dynamics, *Nature*, *451*, 279–283.
- Zhao, C., D. Ye, D. Wei, B. Chen, and D. Liu (1994), *Tertiary in Petroliferous Regions of China*, Oil Ind. Press, Beijing.
- Zhou, L., H. Friis, and M. L. K. Poulsen (2015), Geochemical evaluation of the Late Paleocene and Early Eocene shales in Siri Canyon, Danish–Norwegian Basin, *Mar. Pet. Geol.*, *61*, 111–122.